Effect of joint gap on the quality of laser beam welded near-β Ti-5553 alloy with the addition of Ti–6Al–4V filler wire

T. Shariff · X. Cao · R. R. Chromik ·
P. Wanjara · J. Cuddy · A. Birur

Abstract Ti–5Al–5V–5Mo–3Cr (Ti-5553) sheets were welded using a Nd: YAG laser system and Ti–6Al–4V filler wire. The effect of joint gap on weld geometry, defects, microstructure, and hardness was investigated. Fully penetrated welds up to a joint gap of 0.5 mm were produced. The two main defects observed were porosity and underfill. The addition of filler wire reduced underfill but increased porosity, especially at large joint gaps. The fusion zone (FZ) microstructure at low joint gaps consisted of retained β with a dendritic morphology. At a joint gap of 0.3 mm, regions of orthorhombic α'' martensite were observed in the weld zone which increased in proportion as the joint gap increased from a volume percentage of 4.9% at 0.3 mm to a volume percentage of 44% at 0.5 mm. Despite the differences in microstructure with increasing joint gap, the FZ hardness remained relatively constant for all joint gaps evaluated.

Introduction

Titanium alloys offer a combination of some excellent properties, particularly high specific strength and good corrosion resistance. As a result, titanium alloys have been very attractive to the aerospace industry for reducing operating costs through lower weight and less maintenance [1]. To this end, it has been reported that the use of titanium-based alloys in Airbus aircrafts has risen from 5% by weight for the earlier models to almost 10% in Airbus A380 [2]. The Boeing 777 airframe uses approximately 10% titanium alloys out of which the high strength β alloy Ti–10V–2Fe–3Al (Ti-10-2-3) has outweighed the most commonly used α/β alloy, Ti–6Al–4V [3].

In recent years, both Boeing and Airbus have announced that Ti-10-2-3 will be replaced by a new near-β alloy, Ti–5Al–5V–5Mo–3Cr (Ti-5553), for landing gear assemblies [4]. Ti-5553, a variation of the Russian alloy VT22 [5], is a heat-treatable titanium alloy characterized by high strength ($\sim$1250 MPa at room temperature for certain microstructures) and high cycle fatigue properties compared to Ti–6Al–4V [6]. It is also applicable for thick sections due to its deep hardenability and offers a wider processing window than Ti-10-2-3 [4, 7]. Ti-5553 contains β stabilizing elements such as V, Mo, and Cr which depress the β-transus temperature to an average value of 856 °C [5]. The high strength of Ti-5553 results from the precipitation of fine α-phase particles during low temperature aging performed after solution treatment below the β-transus temperature. The degree of strengthening is dependent on the size, morphology, and volume fraction of the α-phase particles.

Laser beam welding has been used in recent studies to weld Ti–6Al–4V and commercially pure Ti [8–13]. While Ti-5553 has numerous forecasted applications, very little is known of its weldability. This issue needs to be addressed if Ti-5553 is to gain wider implementation in the near future. Laser beam welding offers many advantages compared to conventional fusion welding, which includes low and precise heat input, deep and narrow fusion zone (FZ), small heat-affected zones (HAZs), low thermal distortion,

T. Shariff (✉) · X. Cao · P. Wanjara
Aerospace Manufacturing Technology Center, Institute
of Aerospace Research, National Research Council Canada,
5145 Decelles Avenue, Montreal, QC H3T 2B2, Canada
e-mail: tasneem.shariff@mail.mcgill.ca

T. Shariff · R. R. Chromik
McGill University, 3610 University Street, Montreal,
QC H3A 2B2, Canada

J. Cuddy · A. Birur
Standard Aero Limited, 33 Allen Dyne Rd., Winnipeg,
MB R3H 1A1, Canada

and high productivity. Welding can be conducted either autogenously (without filler metal) or with filler metal. Although autogenous welding has many advantages, the addition of filler metal helps to ease the strict joint fit-up requirement for laser welding. It also allows for the tailoring of weld properties by modifying the FZ composition [14].

This technique has been successfully developed to produce high quality and reproducible welds for Ti–6Al–4V components [1]. The purpose of this study was to investigate the joint gap tolerance for the new Ti-5553 alloy using a 4 kW continuous wave (CW) Nd: YAG laser and Ti–6Al–4V filler wire. The weld quality was determined in terms of surface properties, microstructure, defects, and hardness.

Experimental procedure

The Ti-5553 material, received in ingot form, was sectioned to obtain weld coupons of 76 mm in length × 38 mm in width × 3.1 mm in thickness. The composition of the alloy is as follows: 5.9% Al, 5.9% Mo, 4.6% V, 3.1% Cr, and 0.3% Fe (alloy composition is in wt% unless indicated otherwise.). Prior to welding, the weld coupons were solution treated at 815 °C for 45 min in vacuum followed by an argon quench. The samples were then aged at 621 °C for 8 h followed by an argon quench. The furnace temperature uniformity was ± 8 °C. The faying surfaces and the surrounding areas of each blank were brushed and then cleaned with methanol to remove surface oxides and any contaminants prior to clamping and welding. Butt welds, 76 mm in seam length, were welded using a 4 kW CW Nd: YAG laser system (manufactured by TRUMPF, Germany). In all cases, welding was only conducted on one side of the coupons. A collimation lens of 200 mm, focal lens of 150 mm, and a fiber diameter of 0.6 mm were employed to produce a laser beam with a focal spot diameter of approximately 0.45 mm. High purity argon at a flow rate of 23.6 L/min was used to shield the top surface of the work-piece. The bead trail on the top surface and the bottom of the work-piece were shielded using helium at a flow rate of 66.1 L/min. A laser power of 4 kW, defocusing distance of −1 mm (i.e., below the top surface of the sheet by 1 mm), and welding speed of 3.0 m/min were utilized. The joint gap was varied from 0 (no filler wire used) to 0.6 mm. A joint gap of 0.6 mm yielded a lack of penetration, hence the results of the 0.6 mm joint gap are not discussed. Ti–6Al–4V filler wire with a specification of AMS 4956A ELI and a nominal diameter of 1.14 mm was fed at a 30° angle relative to the top surface of the sheet. The feed rate of the filler wire was calculated by using the volume flow rate constancy equation:

$$\text{Wire feed rate} = \frac{v \times t \times b}{(\pi/4)d^2}, \tag{1}$$

where v is the welding speed (m/min), t is the sheet thickness (mm), b is the gap size (mm), and d is the diameter of filler wire (mm). The wire feed rates were 0, 0.9, 1.8, 2.7, 3.6, and 4.5 m/min for joint gaps at 0 (no gap), 0.1, 0.2, 0.3, 0.4, and 0.5 mm, respectively.

After welding, the coupons were examined by X-ray radiography to detect any cracks and/or porosity in the weld regions. The surface quality of all laser welds was visually evaluated and macroscopically recorded using an Olympus SZ40 stereoscope. For the examination of the transverse section and microstructure of the welds, three samples were cut from each joint and then mounted using cold-setting epoxy resin. The samples were prepared using standard metallographic techniques with a final polishing step of 0.04 μm colloidal silica mixed with 10% hydrogen peroxide to produce a mirror-like finish. Etching to reveal the microstructure was accomplished by dipping the polished welds into Kroll's reagent (1–3 mL HF + 2–6 mL HNO_3 + 100 mL H_2O) for approximately 10 s. Microstructural examination was carried out using an inverted optical microscope (Olympus GX71) equipped with digital image analysis software (AnalySIS Five). The microhardness profiles across the welded joints were measured at a testing load of 500 g and a dwell time of 15 s using a Vickers microindentation machine (StruersDuramin A300). For each weld condition, three hardness profiles across the weld joint near the top, center, and root height of the joint were made with an indent interval of 0.3 mm.

Results and discussion

Weld beads

The weld surfaces (not shown) were uniform and silver colored along the weld seam. No significant surface defects such as cracks and porosity were observed. Figure 1 shows typical transverse sections of the welds. Full joint penetration of the titanium sheets was accommodated at joint gaps ranging from 0 to 0.5 mm. There was a lack of penetration at a joint gap of 0.6 mm. For this reason, joint gaps greater than 0.6 mm were not investigated in this study. The maximum joint gap accommodated (i.e., 0.5 mm) was almost equal to the beam diameter of the Nd: YAG laser used (i.e., approximately 0.49 mm at a defocusing distance of −1 mm).

Li et al. have shown that the color of commercially pure titanium changes from silver to dark blue with an increasing amount of oxygen in the argon shielding gas [10]. However, it was also pointed out that it was not

Fig. 1 Micrographs obtained by light optical microscopy for transverse sections of 3.1-mm thick joints in Ti-5553 with different gap values at the interface

(a) 0 mm (no gap)

(b) 0.1 mm

(c) 0.2 mm

(d) 0.3 mm

(e) 0.4 mm

(f) 0.5 mm
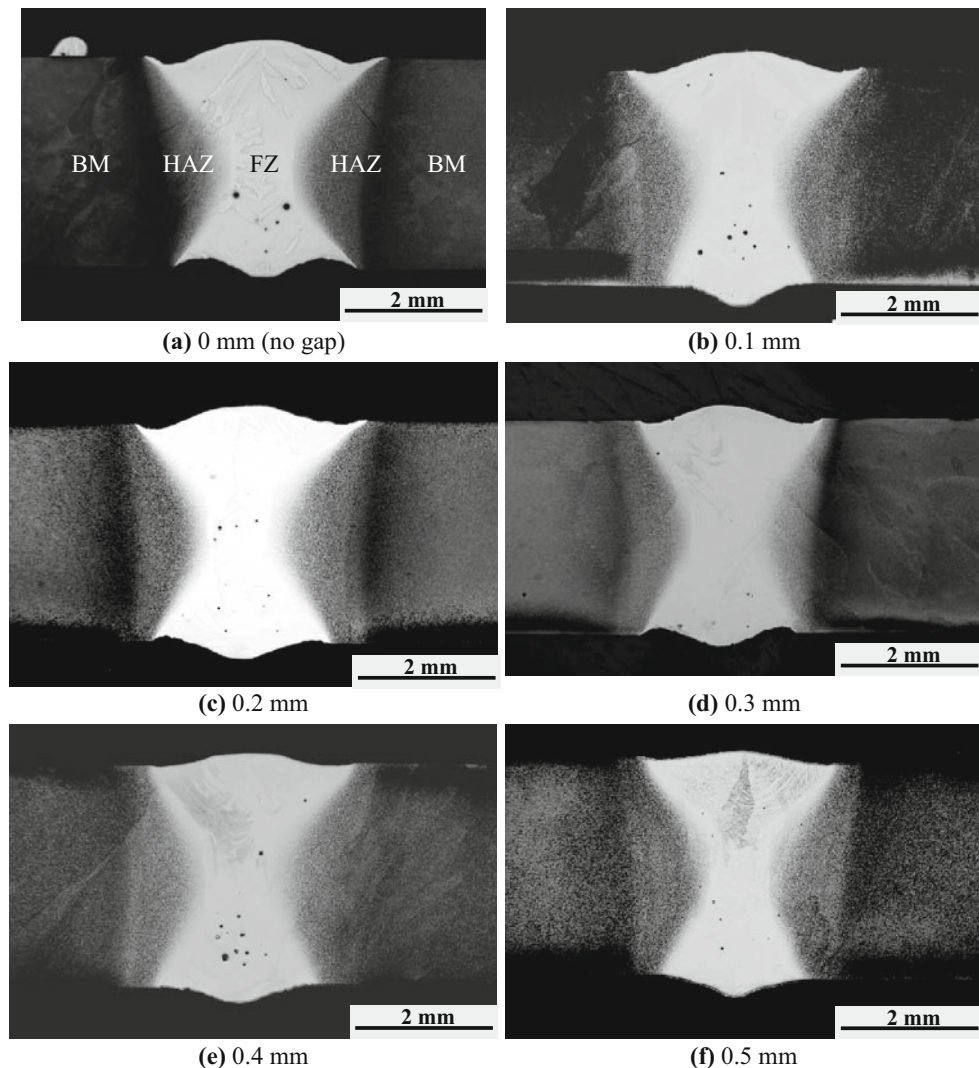
suitable to rely on the surface color as a measure of the shielding deficiency since the color sequence would tend to repeat itself with increasing oxidation thickness [10].

The welds produced in this study were characterized by an "hourglass" shape for which the top and bottom FZ widths were greater than the middle FZ width. The hourglass shape, which is characteristic of deep penetration welding, is usually attributed to the flow of molten metal due to differences in surface tension and buoyancy [15, 16]. The strong stirring forces in the weld pool are driven by Marangoni type forces which result from the variation in surface tension with temperature [15, 16]. The metal flows from the high temperature regions to the low temperature regions, leading to an expansion of the FZ at the top and bottom.

There are three distinguishable regions in the welds which are commonly termed the FZ, HAZ, and base metal (BM). The area and width of the FZ and the HAZ were measured by means of an image analysis software and the results are plotted in Fig. 2. It was found that the maximum

top width occurred at zero joint gap and decreased with increasing gap size. No significant changes in other joint dimensions were observed over the gap range from 0 to 0.5 mm.

Defects

The most common defects observed were underfill and porosity as seen in Fig. 1. No welding cracks were observed in the microstructural cross-sections of the welds or detected using X-ray examination. All of the porosity observed in the joints was spherical in shape indicating that they were most likely gas porosity. The results obtained from X-ray examination are indicated in Table 1. It was found that the highest average pore size was about 0.25 mm. However, the highest average pore size measured from the optical micrographs using the analysis software was much smaller than that determined by X-ray radiography, as the latter permits the examination of the entire weld length (greater sampling volume) whereas the
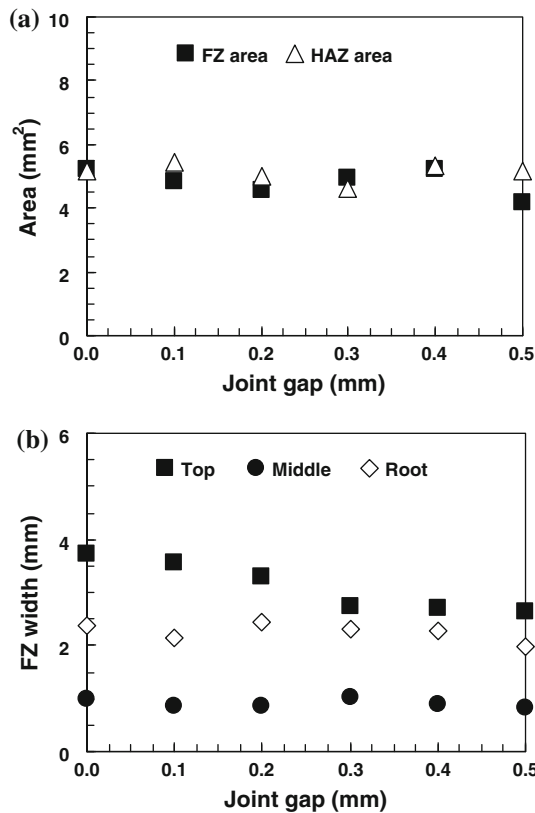
Fig. 2 Effect of joint gap on the **a** FZ and total HAZ areas and **b** FZ widths

Table 1 Average porosity size determined by radiography and optical microscopy

Gap (mm)	Wire feed rate (m/min)	Avg. pore size by X-ray (mm)	Avg. pore size by optical (mm)	Max pore diameter by optical (mm)
0.0	0	0.13	0.02	0.04
0.1	0.90	0.13–0.25	0.06	0.12
0.2	1.86	0.13	0.05	0.05
0.4	3.66	0.13–0.25	0.05	0.14
0.5	4.50	0.13–0.25	0.10	0.19

former is limited by the number of transverse sections sampled from the weld. In addition, radiographs are more reliable at detecting macroporosity (i.e., porosity that may be resolved using the visible eye typically as small as 0.1 mm) within the weld while the detection of microporosity requires optical microscopy. The effect of joint gap on the total porosity area, calculated as the total pore area over the FZ from measurements on optical micrographs, is shown in Fig. 3a. The maximum pore area percentage was produced at joint gaps of 0.4–0.5 mm. Similar trends for porosity versus joint gap were obtained for laser-welded Ti–6Al–4V alloy [17].

Fig. 3 Effect of joint gap on **a** porosity and **b** underfill area

There are several possible explanations for the origin of the porosity in welded joints. Porosity in titanium welds is generally attributed to hydrogen [18]. The solubility of hydrogen in titanium alloys usually decreases with increasing temperature [18]. One of the sources for hydrogen can be from filler wire and this is most likely the case for the 0.4 and 0.5 mm joint gaps. With increasing joint gap, more filler wire is used (as demonstrated in the volume constancy relation given by Eq. 1) and hence there are more opportunities for hydrogen contamination. In addition to hydrogen, metal vapor, shielding gas, or air may also contribute to the gas porosity [19]. The shielding gas or air may be entrapped into the weldments due to surface turbulence. The metal vapors are most likely from the keyholes or due to the evaporation of the alloying elements.

Underfill at the top and root surfaces was commonly observed in the weld joints. As seen in Fig. 1, underfill appears as depressions on the top or root surface extending below the adjacent surface of the HAZ. Figure 3b illustrates the effect of joint gap on the underfill area. The maximum underfill area for both the top and root surface of the weld was observed at the 0 mm joint gap where no filler wire was used. The minimum underfill was obtained at joint gaps of 0.4 and 0.5 mm. In general, underfill

decreases with increasing joint gap indicating that the use of filler wire can significantly reduce the underfill defect.

There are two possible mechanisms for underfill formation: (1) the expulsion and/or evaporation of the molten metal which is usually dominant at lower welding speeds and/or high laser power and (2) inability for the molten metal to refill the depressions at high welding speeds. It is accepted that the addition of filler wire can reduce the underfill since it can refill the depressions that are produced during welding [20]. At the larger joint gap values (i.e., 0.4 and 0.5 mm in this study), the underfill is smaller, mainly due to more laser energy loss that leads to less expulsion and/or evaporation of the molten metal. It is important to avoid or minimize the underfill defect since it has a negative impact on the welding quality. Underfill reduces the sheet thickness and creates stress concentrations, causing a decrease in fatigue life and tensile strength of the joints [17]. According to the fusion welding specification for aerospace applications (AWS D17.1), a maximum underfill depth of $0.07T$ (where T is the thickness or 3.1 mm in this study) is acceptable for Class A welds. Over a joint gap range of 0–0.5 mm, a maximum underfill depth of approximately 0.12 mm was found at 0 gap. Consequently, the Ti-5553 laser welds obtained in this study have an underfill depth below 0.22 mm $(0.07T)$ and satisfy the Class A requirements for underfill.

From the defects described above, there is a trade-off between porosity and underfill over the joint gap range of 0–0.5 mm. Although underfill is significantly reduced as the joint gap is increased from 0 to 0.5 mm, the opposite effect is observed for porosity. Apart from optimizing laser parameters (i.e., laser power, welding speed, and defocusing distance) to reduce defects such as porosity and underfill, it is necessary to find a joint gap that sufficiently balances the effect of both underfill and porosity in the case when filler wire is used. The optimum gap values are probably in the intermediate level (around 0.2–0.3 mm), which is consistent with the recommendation by Dilthey et al. [14] to select a joint gap that is <10–15% of the sheet thickness (i.e., <0.3–0.5 mm for the 3.1 mm thickness

applied in this study). This was also consistent with the results obtained in laser beam-welded Ti–6Al–4V alloy [21].

Microstructure

Figure 4a and b shows an optical and SEM micrograph of the Ti-5553 BM, respectively. The bimodal microstructure of the BM consists of globular (or equiaxed) primary α particles in a β matrix with fine secondary α platelets which are evolved during low temperature aging. The volume percentage of the primary α globular phase in the BM is approximately 20 ± 5% (average of 20% with a standard deviation of 5%) and the average particle diameter is approximately 2.1 ± 0.2 μm.

The as-welded structure at 0 mm gap without the use of Ti–6Al–4V filler wire is shown in Fig. 5. No α phase (including globular and platelet) was observed in the FZ. The FZ, which experiences temperatures above the liquidus of the alloy, consisted entirely of the metastable β phase that is formed during rapid cooling after laser welding. Coarse columnar β grains in the FZ epitaxially grow directly from the semi-melted grains in the near HAZ toward the central weld pool opposite the heat extraction direction, as seen in the optical micrograph in Fig. 5a and b. Within the FZ, a cellular dendritic solidification microstructure was observed (Fig. 6c). Some prior β grains are clearly identified in Fig. 5a.

The HAZ revealed two distinct regions as seen in Fig. 5b, which are termed the near HAZ and the far HAZ [22]. The near HAZ is a very narrow region adjacent to the FZ which consists entirely of the β phase, with no other observable structures. Since the temperature experienced is below the liquidus temperature but above the β transus temperature, both the globular and platelet α phase in the near HAZ is fully dissolved during laser welding. In contrast, the far HAZ experiences temperatures below the β transus and consists of both the α (globular and platelets) and β phases. Figure 6 illustrates the microstructures in the far HAZ at several locations starting from a region close to

Fig. 4 Optical (*left*) and SEM (*right*) micrographs of the base material showing bimodal α morphologies in a β matrix

Primary globular α

Secondary platelet α

25μm
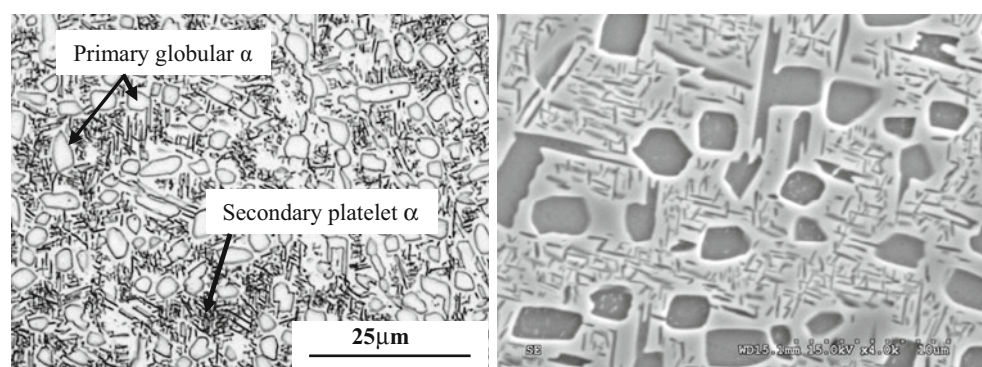
Fig. 5 Overview of microstructures for 0 mm joint gap (no filler wire added) (**a**) transverse section, (**b**) heat-affected zone/fusion zone with DIC, and (**c**) fusion zone with DIC
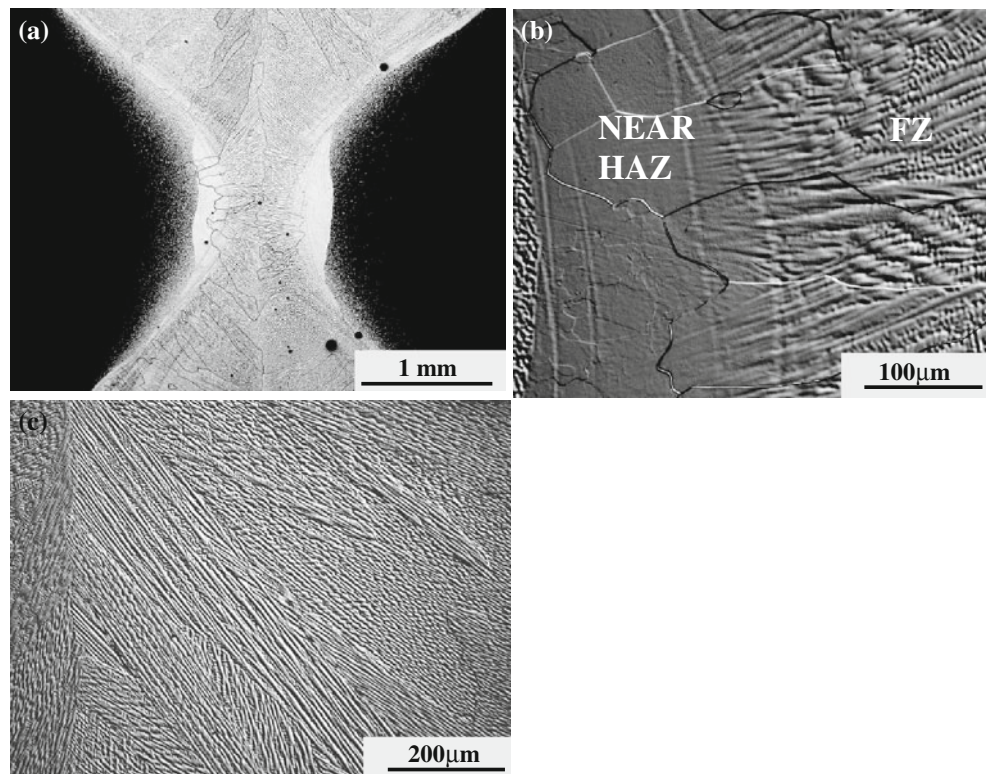
Fig. 6 Series of optical micrographs at various locations in the far HAZ for a weld obtained at a welding speed of 2.25 m/min and a defocusing distance of −1 mm

(a) overview

(b) region 1 of far HAZ

(c) region 2 of far HAZ

(d) region 3 of far HAZ
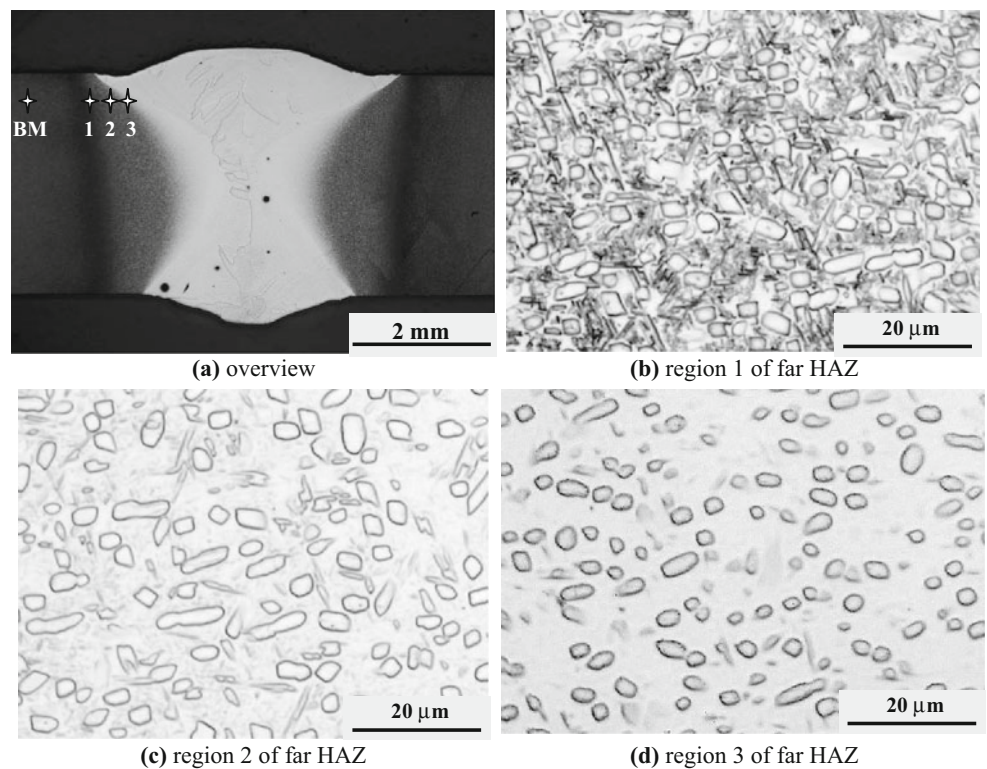
the BM/HAZ interface (Fig. 6b) to an area close to the far HAZ/near HAZ interface (Fig. 6d). It can clearly be seen that dissolution of the α phase (both primary and secondary) progressively occurs in the HAZ, where the

temperatures experienced are high enough for the solid-state dissolution to occur.

Figure 7 shows the effect of joint gap on the FZ microstructure. For joint gaps ranging from 0 to 0.2 mm, the filler

Fig. 7 Effect of joint gap on the microstructure in the fusion zone

(a) 0 mm

(b) 0.1 mm

(c) 0.2 mm

(d) 0.3 mm

(e) 0.4 mm

(f) 0.5 mm
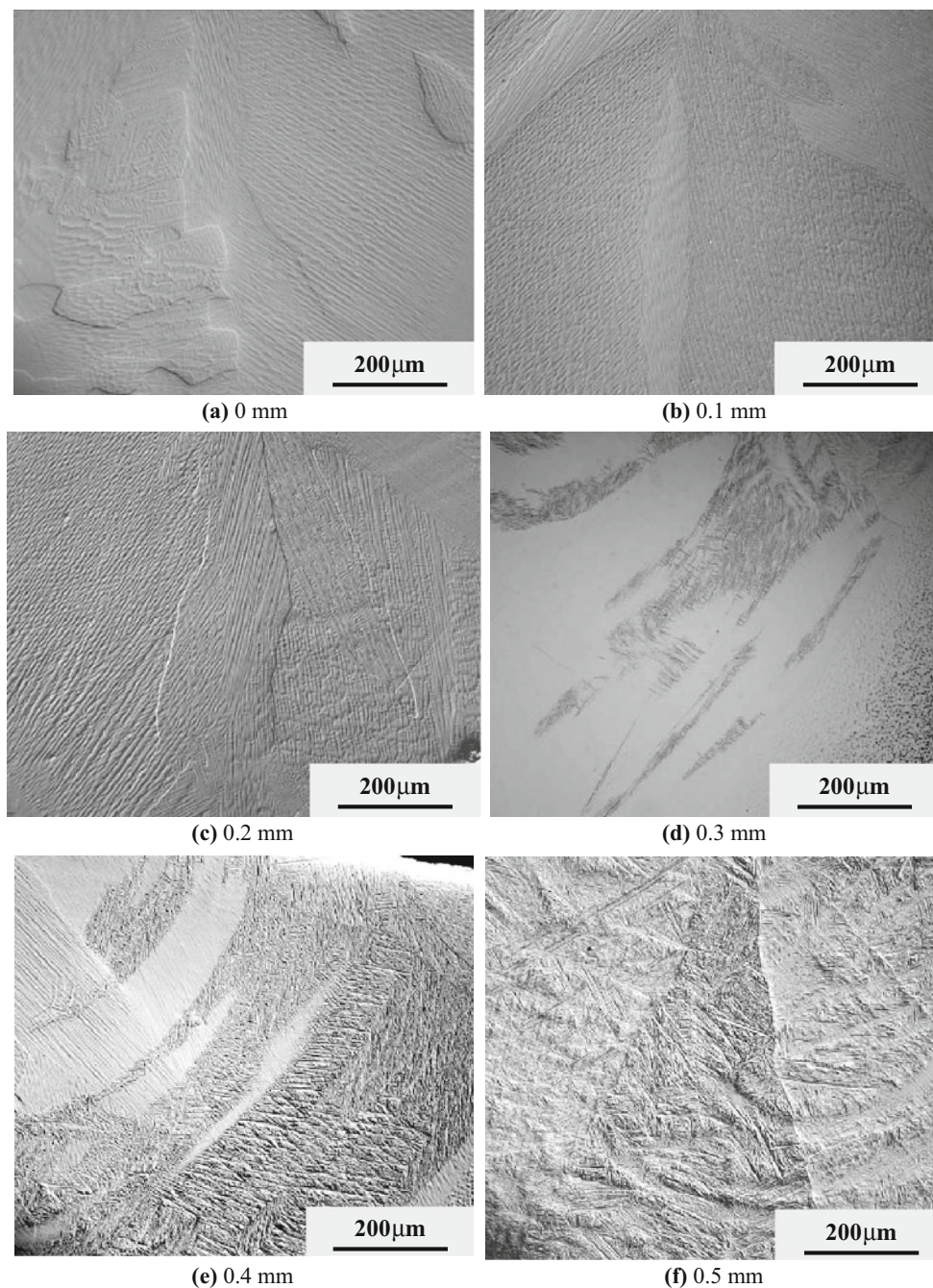
wire was completely intermixed with the melted BM and thus the microstructure in the FZ consisted of the retained β phase with a cellular dendritic morphology as was the case for the weld conducted without the use of filler wire at 0 mm joint gap. As the joint gap was increased above 0.2 mm, distinct regions of martensite appeared in the FZ due to incomplete mixing of the filler wire with the melted BM (i.e., macrosegregation). The martensitic structure was characterized by plates with extensive internal twinning as seen in Fig. 8. The area of martensite in the FZ was measured directly from the optical micrographs and the results are plotted in Fig. 9. The amount of Ti–6Al–4V filler wire fed

into the system was calculated from the volume constancy relation (Eq. 1) and is also plotted in Fig. 9. It is observed that the proportion of martensite in the FZ increased as a greater quantity of Ti–6Al–4V filler wire was added until reaching an amount of approximately 44% at a joint gap of 0.5 mm. At this joint gap, it is observed that the amount of martensite measured is greater than the amount of the filler wire added into the system. This is due to the error associated with the measurement of the martensite area directly from the optical micrograph since there might be small amounts of the β phase present between the martensitic bands that are not easily excluded during the measurement. It has been reported

Fig. 8 High magnification optical images showing the regions of martensite and retained β at joint gaps ranging from 0.3 to 0.5 mm

(a) 0.3 mm

(b) 0.4 mm

(c) 0.5 mm
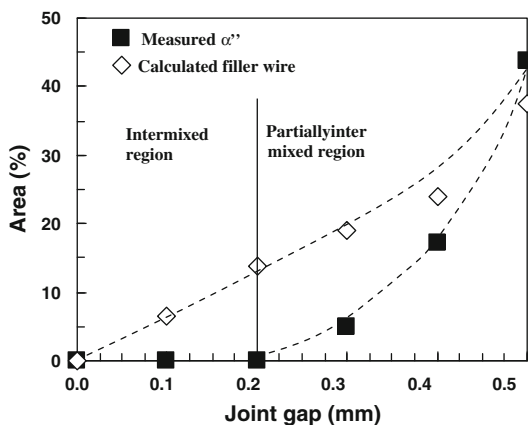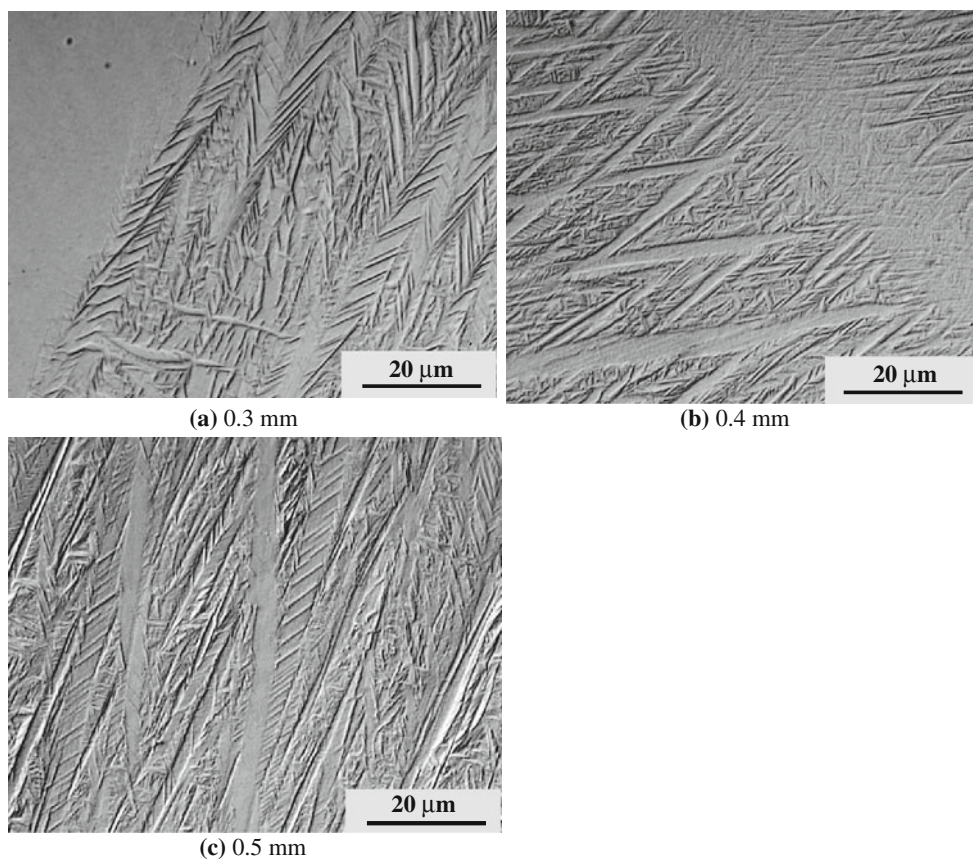
Fig. 9 Influence of joint gap on the amount of martensite observed in the fusion zone with respect to the quantity of the filler wire added

that macrosegregation has a negative impact on weld quality since it may result in hydrogen cracking, corrosion, and stress corrosion cracking within the weld metal [23]. However, no cracks were observed in this study.

Hardness

Vickers microindentation hardness profiles were made across the top, middle, and bottom of each weld joint. A
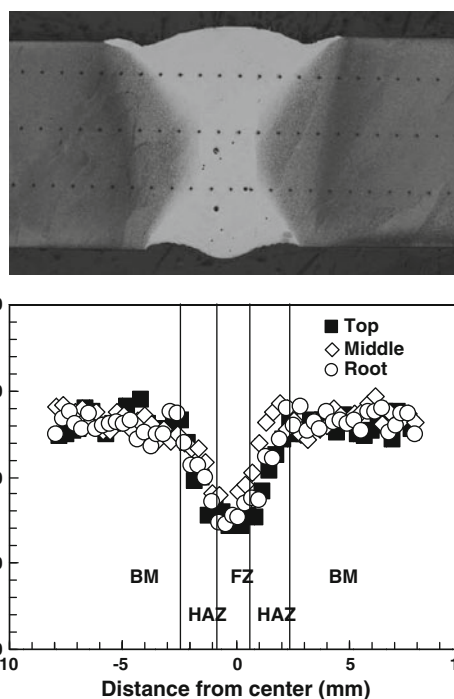
Fig. 10 Hardness profile across the weld at 0.1 mm joint gap

typical microindentation hardness profile for a 0.1 mm joint gap is shown in Fig. 10. The variation in microstructure from the BM to the FZ during laser welding is
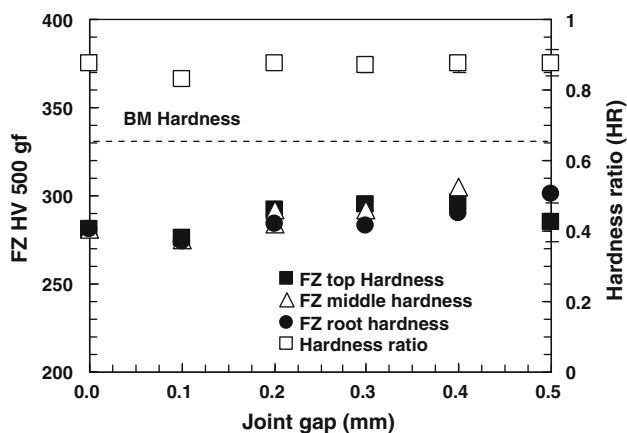
Fig. 11 Effect of joint gap on the fusion zone hardness

well reflected in the hardness distribution of the weld joint. A decrease in hardness from an average of 330 ± 6 HV in the BM ($\alpha + \beta$ structure) to a hardness of 286 ± 9 HV in the FZ (retained β structure) is observed and represents a 13% decrease. The hardness reduction was correlated with the dissolution of the α phase (including both globular and platelet) in the HAZ. The strengthening mechanism in metastable β titanium alloys relies heavily on α phase precipitation (both globular and platelets) for which the volume fraction, morphology, and location strongly influence the mechanical properties of these alloys [24].

Figure 11 shows the effect of joint gap on the average FZ hardness at the top, middle, and root of the weld. The hardness ratio is calculated by dividing the FZ hardness by the BM hardness. It can be noticed that there is no significant variation of the FZ hardness with increasing joint gap (ranging from approximately 280 HV to 300 HV), despite the variation in the amount of martensite.

The hardness of the FZ during Ti–6Al–4V laser welding has been measured to be approximately 412 ± 10 HV for a single pass 1-mm thick joint consisting of a needle-like hexagonal α' martensitic phase that is formed when quenched below the β transus [13]. The hardness values measured for the Ti-5553 welds with the use of Ti–6Al–4V filler wire (280–300 HV in the FZ), are far lower than that for the α' martensite (412 HV), even for the weld produced at a joint gap of 0.5 mm, which reveals an amount of martensite around 40%. One possibility is that the martensite obtained in the FZ may not be the common α', but is rather a softer and more ductile orthorhombic α'' martensite which is thought to have similar lattice correspondence with the β phase [25]. The hardness reported for orthorhombic α'' martensite (275–295 HV 200 g) is close to that of the retained β with negligible hardness differences [26]. The ductility is relatively high and the strength is relatively low for the alloys quenched to α'' martensite [25]. The type of the martensite formed on quenching is mainly

determined by the composition of the alloy [27]. In a study of a near β alloy Ti–10V–2Fe–3Al, the margin for the formation of either retained β or orthorhombic martensite for GTA welding was set at an alloy chemistry of approximately 4–4.5 wt% Al and 10–10.5 wt% β stabilizer (i.e., V, Mo, Cr) [27]. A decrease from this amount of β stabilizers promoted the decomposition of β to martensite α'', whereas an increase favored the retention of the β phase. As observed in this study, the martensitic microstructure was usually located in the Ti–6Al–4V filler wire regions. Due to the incomplete and non-uniform mixing of the BM with the filler wire, only a relatively small amount of the BM (Ti-5553) can mix with the melted Ti–6Al–4V filler wire. If, for example, we consider a volumetric proportion of 1:4 for Ti-5553 to Ti–6Al–4V in the martensite region, an alloy with a nominal composition of Ti–5.8Al–4.2V–1Mo–0.6Cr is obtained, i.e., the total amount of the β stabilizer is well below the threshold (10–10.5%). Thus, the local chemistry seems to favor to the formation of martensite α'' in some local regions of the FZ. However, no definite conclusions can be made on the martensite obtained and compositional analysis has yet to be investigated.

Conclusions

Ti-5553 sheets with a thickness of 3.1 mm were welded using a 4 kW Nd: YAG laser system and Ti–6Al–4V filler wire. The effect of joint gap on the surface quality, weld geometry, defect characteristics, microstructure, and hardness was investigated and the following conclusions are reached:

(1) Butt joints can be welded with full penetration up to a maximum joint gap of 0.5 mm.

(2) No cracks are observed in the welds. The most common defects observed are porosity and underfill. The porosity area is the greatest for larger joint gaps but remains <1% of the total FZ area. In contrast, the underfill defect is significantly reduced with the addition of filler wire.

(3) The BM exhibits a bimodal microstructure with α globular precipitates and fine α platelets in a retained β matrix. Both α precipitates (primary and secondary) are found to dissolve in the HAZ. The FZ at joint gaps <0.2 mm shows a relatively uniform microstructure, consisting of a retained β phase with a cellular dendritic morphology. At a joint gap ranging from 0.3 to 0.5 mm a banded microstructure containing both martensite and retained β is observed, with the amount of martensite increases with increasing joint gap and the associated addition of the filler wire.

(4) Compared with the BM, a 13% decrease in hardness is observed in the HAZ due to the dissolution of the strengthening α precipitates (both globular and plate-like).

(5) In spite of the presence of martensite at large joint gaps due to the use of the Ti–6Al–4V filler wire, no significant variations are seen in the FZ hardness compared to those consisting entirely of the retained β phase. Since the martensite and the β phase have comparable hardness, the values of the hardness dip in the FZ were comparable for different gap widths.

References

1. Boyer RR, Cotton JD, Slattery KT, Weber GR (2008) Adv Mater Process 166:25
2. Rendigs K-H (2004) Titanium products used at AIRBUS. Paper presented at the Ti-2003 Science and Technology, Weinheim, Germany
3. Lütjering G, Williams JC (2003) Titanium. Springer, Berlin, Heidelberg
4. Boyer RR, Briggs RD (2005) J Mater Eng Perform 14(6):681
5. Fanning JC, Boyer RR (2005) J Mater Eng Perform 14(6):788
6. Veeck S, Lee D, Boyer R, Briggs R (2005) J Adv Mater 37(4):40
7. Moiseyev VN (2006) Titanium alloys: Russian aircraft and aerospace applications. CRC Press, Boca Raton
8. Buddery A, Kelly P, Drennan J, Dargusch M (2011) J Mater Sci 46:2726. doi:10.1007/s10853-010-5145-5
9. Huang H-H, Lin S-C, Lee T-H, Chen C-C (2005) J Mater Sci 40:789. doi:10.1007/s10853-005-6325-6
10. Li X, Xie J, Zhou Y (2005) J Mater Sci 40:3437. doi:10.1007/s10853-005-0447-8
11. Shi Y, Zhong F, Li X, Gong S, Chen L (2007) J Mater Sci 42:6651. doi:10.1007/s10853-007-1524-y
12. Vaidya WV, Horstmann M, Ventzke V, Petrovski B, Kocak M, Kocik R, Tempus G (2010) J Mater Sci 45:6242. doi:10.1007/s10853-010-4719-6
13. Cao X, Jahazi M (2009) Opt Lasers Eng 47:1231
14. Dilthey U, Fuest D, Scheller W (1995) Opt Quant Electron 27:1181
15. DebRoy T, David SA (1995) Rev Mod Phys 67(1):85
16. Steen WM (1998) Laser material processing, 2nd edn. Springer, London
17. Cao X, Debaecker G, Poirier E, Marya S, Cuddy J, Birur A, Wanjara P (2009) Effect of joint gap in Nd: YAG laser welded Ti–6Al–4V (paper no. 157). Paper presented at the ICALEO, Orlando, FL
18. Mitchell DR (1982) Weld J 61:157s
19. Khaled T (1994) J Mater Eng Perform 3(3):419
20. Cao X, Wallace W, Poon C, Immarigeon J-P (2003) Mater Manuf Process 20(5):1
21. Cao X, Debaecker G, Poirier E, Marya S, Cuddy J, Birur A, Wanjara P (2009) Effect of joint gap on Nd: YAG laser welded Ti–6Al–4V (paper P157). Paper presented at the ICALEO 2009, Orlando, FL, Nov 2–5, 2009
22. Short AB (2009) Mater Sci Technol 25(3):309
23. Yang YK, Kou S (2010) Sci Technol Weld Join 15(1):15
24. Clement N, Lenain A, Jacques PJ (2007) J Miner Met Mater Soc 59(1):50
25. Moiseev VN, Polyak EV, Sokolova AY (1975) Met Sci Heat Treat 17(8):687
26. Liu PS, Hou KH, Baeslack WA III, Hurley J (1993) In: Eylon D, Boyer R, Koss DA (eds) Beta titanium alloys in the 1990's: proceedings of a symposium on beta titanium alloys sponsored by the titanium committee of TMS, Denver, CO, 1993. TMS (The Minerals, Metals & Materials Society), pp. 383–393
27. Liu PS, Baeslack WA, Hurley J (1994) Weld J 73(7)